

Coexistence of spin-1/2 and spin-1 Dirac-Weyl fermions in the edge-centered honeycomb lattice

Zhihao Lan,¹ Nathan Goldman,² and Patrik Öhberg¹

¹*SUPA, Department of Physics, Heriot-Watt University, EH14 4AS, Edinburgh, United Kingdom*

²*Center for Nonlinear Phenomena and Complex Systems - Université Libre de Bruxelles, 231, Campus Plaine, B-1050 Brussels, Belgium*

We investigate the properties of an edge-centered honeycomb lattice, and show that this lattice features both spin-1/2 and spin-1 Dirac-Weyl fermions at different filling fractions f ($f = 1/5, 4/5$ for spin 1/2 and $f = 1/2$ for spin 1). This five-band system is the simplest lattice that can support simultaneously the two different paradigmatic Dirac-Weyl fermions with half-integer spin and integer spin which also includes a flat band. We further explore the effects of several perturbations on this system, such as a uniform magnetic field, an intrinsic spin-orbit coupling, and charge density waves. Our results demonstrate how these perturbations makes it possible to probe the similarities and differences between the two kinds of relativistic fermions, or even to isolate them individually. We comment also on the possibility to realize such a system using cold atoms.

PACS numbers: 71.10.Fd, 37.10.Jk, 72.25.-b, 73.20.-r

Introduction. In the solid state, matter is typically organized into crystal structures. The mathematical models for describing different materials are consequently based on lattices where the electrons are trapped in periodic structures. The understanding of the equilibrium and transport mechanisms in such systems also forms our understanding of many fundamental effects and indeed technological applications of today. Recently emergent phenomena such as quasi-relativistic effects in non-relativistic settings have proven to be important in this respect. Most notably graphene together with topological insulators [1, 2] are prominent examples of this. The emergent quasi-relativistic fermions in graphene and topological insulators are two-spinor massless Dirac fermions, but it has also been suggested that in more exotic lattices such, as the \mathcal{T}_3 lattice [3] and the line-centered-square Lieb lattice [4–6], the emergent massless fermions are in fact pseudospin-1 objects which also involves a flat band. Also Dirac-Weyl fermions with arbitrarily large spin has been studied based on fermionic atoms trapped in optical super lattices [7, 8].

In this paper we explore a different direction: can we find a single setup where several different kinds of Dirac-Weyl fermions can coexist in the same lattice? This is an intriguing question. Such a “material” should have remarkably versatile properties as far as density dependent effects are concerned, as we will show in this paper. Our initial efforts to solve this problem is motivated by the study of Lieb lattices [4–6], where additional lattice sites on the edges of the square lattice gives rise to a flat band. From this inspiration, we expect that when introducing additional lattice sites to the edges of the standard honeycomb lattice [1], which we refer to as the *edge-centered honeycomb* (ECH) lattice in the following, a flat band should also emerge, thus giving both spin-1/2 and spin-1 Dirac-Weyl fermions. This is indeed what we have found in this study. We also note that the next-nearest-neighbor (NNN) hopping in this ECH lattice produces the well-known Kagome lattice [9], thus the ECH lattice interpolates between several well researched lattices, such as honeycomb, Lieb and Kagome lattices. Furthermore, we investigate the response of the system to perturbations such as a uniform magnetic field, a Haldane-type spin-orbit coupling,

and a charge density wave (CDW). We demonstrate how these perturbations allow us to probe the similarities and differences between the two kinds of relativistic fermions. This five-band model turns out to be a minimal model that can support simultaneously the two different paradigmatic Dirac-Weyl fermions at the lowest spin level, i.e., spin-1/2 without flat band and spin-1 with a flat band.

ECH lattice with spin-1/2 and spin-1 Dirac-Weyl fermions. We are interested in the properties of a fermionic gas trapped in an ECH lattice whose unit cell contains 5 inequivalent sites and are labeled by $\tau = 1, \dots, 5$ as illustrated in Fig. 1 (a). A physical realization of this system could be achieved by trapping fermionic atoms using six lasers, which divide the plane into six sectors of 60° . The corresponding configuration of the laser light fields can be chosen as $\mathbf{E}_1 = E(0, 1)e^{ikx \cdot \mathbf{a}_1}$, $\mathbf{E}_2 = E(\sqrt{3}/2, 1/2)e^{-ikx \cdot \mathbf{a}_2}$, $\mathbf{E}_3 = E(\sqrt{3}/2, -1/2)e^{ikx \cdot \mathbf{a}_3}$, $\mathbf{E}_4 = E(0, -1)e^{-ikx \cdot \mathbf{a}_1}$, $\mathbf{E}_5 = E(-\sqrt{3}/2, -1/2)e^{ikx \cdot \mathbf{a}_2}$ and $\mathbf{E}_6 = E(-\sqrt{3}/2, 1/2)e^{-ikx \cdot \mathbf{a}_3}$, where $\mathbf{x} = (x, y)$ and the vectors $\mathbf{a}_{1,2,3}$ are represented in Fig. 1 (a). In this case, the intensity profile $I(x, y) = |\mathbf{E}_{\text{tot}}(x, y)|^2$ from the total electric field $\mathbf{E}_{\text{tot}} = \sum_i \mathbf{E}_i$ produces a potential landscape as shown in Fig. 1 (c). Alternatively, one can envisage using Spatial Light Modulators for shaping the intensity of a light beam such that the desired minima creates the ECH lattice. Also nanostructured lattice potentials for two-dimensional electron gases [10] can be considered for creating the ECH lattice.

For sufficiently deep lattice sites we can use the tight-binding approximation, which results in the Hamiltonian $H_0 = t \sum_{\langle ij \rangle} c_i^\dagger c_j$, where $c_i^\dagger (c_i)$ is the creation (annihilation) operator at the lattice site i and t is the nearest-neighbor (NN) hopping amplitude. The energy band structure of this system can be obtained from the Hamiltonian in momentum space $H = \sum_{\mathbf{k}} \Psi_{\mathbf{k}}^\dagger H_{\mathbf{k}} \Psi_{\mathbf{k}}$, where $\Psi_{\mathbf{k}} = (c_{1\mathbf{k}}, c_{2\mathbf{k}}, c_{3\mathbf{k}}, c_{4\mathbf{k}}, c_{5\mathbf{k}})^T$ and the non-zero components of the 5×5 matrix $H_{\mathbf{k}}$ are given by $(H_{\mathbf{k}})_{\tau\tau'} = \exp(i\mathbf{k} \cdot \mathbf{v}_{\tau\tau'})$, with $\mathbf{v}_{\tau\tau'}$ the vector connecting two NN sites τ and τ' , e.g. $(H_{\mathbf{k}})_{21} = \exp(i\mathbf{k} \cdot \mathbf{a}_2/2)$ and $(H_{\mathbf{k}})_{24} = 0$. Diagonalizing $H_{\mathbf{k}}$ yields the energy bands $E(\mathbf{k})$ depicted in Fig. 1 (b).

Interestingly, this band structure displays two different regimes. At fillings $f = 1/5$ and $f = 4/5$, two indepen-

dent Dirac cones located at $\mathbf{K}_+ = (\frac{2\pi}{3a}, -\frac{2\pi}{3\sqrt{3}a})$ and $\mathbf{K}_- = (\frac{2\pi}{3a}, \frac{2\pi}{3\sqrt{3}a})$ are present within the first Brillouin zone, which is the same as for the standard honeycomb lattice, where Dirac-like dispersion relations effectively describe spin-1/2 relativistic fermions. At half-filling $f = 1/2$, a flat band is present at the tip of a single Dirac cone located at $\Gamma_0 = (0, 0)$. We find that the wavefunctions associated with the flat band have zero amplitude at the green sites illustrated in Fig. 1 (a), which is compatible with the localization property expected from their infinite effective band mass. This peculiar configuration, involving a flat band and a single Dirac cone, is also present in the Lieb lattice and leads to an effective Hamiltonian describing spin-1 relativistic fermions [4–6]. We see from Fig. 1 (b) that the ECH lattice indeed contains both spin-1/2 and spin-1 relativistic dispersion relations. These two singular and distinct regimes could be reached in a cold-atom realization by simply tuning the atomic filling factor. In order to further explore the distinction between these two relativistic regimes, we show the density of states $\rho(E)$ in Fig. 1 (d). We find that around $E \approx \pm 1.7t$, $\rho(E)$ behaves linearly which is expected for spin-1/2 relativistic fermions. Around $E \approx 0$, the $\rho(E)$ shows a linear behavior and a sharp peak as a consequence of the flat band. As we will demonstrate below, the van Hove singularities located at $E \approx \pm 1.4t$ constitute natural boundaries separating the spin-1/2 and spin-1 relativistic regimes. At this point, let us comment on the interesting fact that the additional (green) lattice sites do not destroy the relativistic properties stemming from the background honeycomb lattice: they rather enrich the quantum properties of the lattice in a non-trivial manner by inducing new relativistic regimes at various fillings.

To demonstrate the above assertion that the low-energy excitations around fillings $f = 1/5, 4/5$ and $f = 1/2$, are indeed Dirac-Weyl fermions of different kinds, we obtain the low-energy effective Hamiltonians describing these excitations around the band-touching points, i.e. \mathbf{K}_\pm at $E \approx \pm 1.7t$ and Γ_0 at $E \approx 0$. Thus, we linearize $H(\mathbf{k})$ near \mathbf{K}_\pm or Γ , and subsequently project onto the subspace associated with the two (for $f = 1/5$ and $f = 4/5$) or three (for $f = 1/2$) touching bands. This leads to

$$h_{\mathbf{p}}^{1/2} = v_{1/2}(p_x\sigma_1 + p_y\sigma_2) \quad \text{at } f = 1/5, 4/5 \quad (1)$$

$$h_{\mathbf{p}}^1 = v_1(p_xS_1 + p_yS_2) \quad \text{at } f = 1/2 \quad (2)$$

where $\mathbf{p} = \mathbf{k} - \mathbf{K}_\pm(\Gamma)$ and $v_{1/2} = \sqrt{3}t/4$, $v_1 = \sqrt{3}t/2$ are the Fermi velocities of the spin-1/2 and spin-1 relativistic fermions. We note here that $v_1 = 2v_{1/2}$ is perfectly compatible with their spin-1 and spin-1/2 nature. While around $f = 1/5, 4/5$, the $\sigma_{1,2}$ are the usual Pauli matrices acting on the two-dimensional subspace associated with the two touching bands, the effective Dirac-Weyl Hamiltonian around $f = 1/2$ features the 3×3 matrices $S_{1,2}$, which fulfill the angular momentum commutation relation $[S_i, S_j] = i\epsilon_{ijk}S_k$. Such an effective Hamiltonian have been shown to describe spin-1 massless Dirac-Weyl fermions, as recently discussed in Refs. [4–

6]. The spin-1/2 and spin-1 Dirac-Weyl fermions therefore do indeed *coexist* in the ECH lattice at different fillings.

Perturbations. We proceed by investigating the effects of various perturbations on the ECH lattice and the two different Dirac-Weyl fermions, highlighting their similar and different natures. We will in particular consider the effect of external magnetic fields, spin-orbit coupling and charge density waves (see Ref. [11] for a review of synthetic gauge field for cold atoms and also Ref. [12] for a recent experimental implementation in optical lattice). Such perturbations will not only provide interesting insights into the physical properties of the ECH lattice, but they will also offer the possibility to distinguish between the different relativistic species in an experiment.

(a) *Synthetic magnetic fields.* When the ECH lattice is subjected to a uniform magnetic flux Φ per plaquette, the energy bulk gaps form a fractal structure in the $E - \Phi$ plane, which consists of two Hofstadter-Rammal butterflies separated by a flat band [13]. When the Fermi energy is exactly located inside such gaps, the Hall conductivity of the system is quantized. A typical sequence of Hall plateaus is shown in Fig. 2. The Hall plateaus clearly evolve differently within the different regimes. Around $f = 1/5, 4/5$, i.e. $E_F \approx \pm 1.7t$, the Hall plateaus feature the *anomalous double step* sequence $\sigma_H^{1/2} = \pm 2(N + 1/2)e^2/h$, where N is an integer. In the vicini-

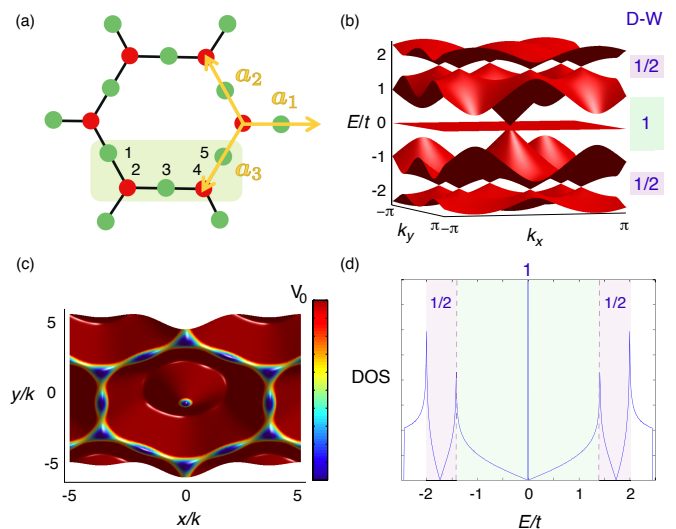


Figure 1: (a) The ECH lattice is characterized by five sites per unit cell. The three NN vectors of the underlying honeycomb structure (red sites) are given by $\mathbf{a}_1 = (1, 0)$, $\mathbf{a}_2 = (-1/2, \sqrt{3}/2)$, $\mathbf{a}_3 = (-1/2, -\sqrt{3}/2)$ while the NN vectors of the ECH lattice by $\mathbf{v}_\mu = \mathbf{a}_\mu/2$, where $\mu = 1, 2, 3$. (b) The energy band structure of the ECH lattice hosts two different kinds of Dirac-Weyl fermions: spin-1/2 at $f = 1/5, 4/5$ and spin-1 at $f = 1/2$. (c) The intensity profile $|I(x, y)|^2$ obtained from a six-laser configuration that would create an ECH lattice for cold atoms. (d). The density of states of the band structure illustrated in (b). The two relativistic regimes (spin-1/2 and spin-1) are separated by van Hove singularities at $E \approx \pm 1.4t$ (cf. vertical dotted lines).

ity of this spin-1/2 regime, each Dirac fermion contributes to the Hall conductivity according to $\sigma_{\text{Dirac}} = (e^2/h)/2$. This is also the case for spin-1/2 Dirac fermions in graphene [14]. Around half-filling, i.e., $E_F = 0$, one observes the characteristic sequence $\sigma_H^1 = \pm N_D N e^2/h$ describing the quantum Hall sequence for spin-integer Dirac-Weyl fermions [7], where N_D is the number of Dirac points crossing the flat band. For integer spin Dirac-Weyl fermions, the absence of the *half-integer anomaly* leads to a zero Hall conductivity plateau. In Fig. 2, we see the characteristic zero Hall conductivity plateau for integer spin Dirac-Weyl fermions and $N_D = 1$, which is in agreement with the fact that a single Dirac cone is present in this spin-1 regime.

Interestingly, a sharp change of behavior occurs at $E_F \approx \pm 1.4t$ located at the van Hove singularities present in the DOS (cf. Fig. 1 (d)), which constitute the boundaries between the $\sigma_H^{1/2}$ and σ_H^1 sequences. We point out that in the standard honeycomb lattice, the van Hove singularities constitute boundaries between relativistic and non-relativistic regimes, which is very different from the result presented here. The Hall conductivity sequence obtained from an ECH lattice subject to a uniform magnetic flux therefore combines the two Hall sequences $\sigma_H^{1/2}$ and σ_H^1 of spin-1/2 and spin-1 Dirac-Weyl fermions respectively. Obtaining the Hall sequence $\sigma_H(E_F)$, such as presented in Fig. 2, would provide a clear signature for the coexistence of spin-1/2 and spin-1 Dirac-Weyl fermions in the ECH lattice.

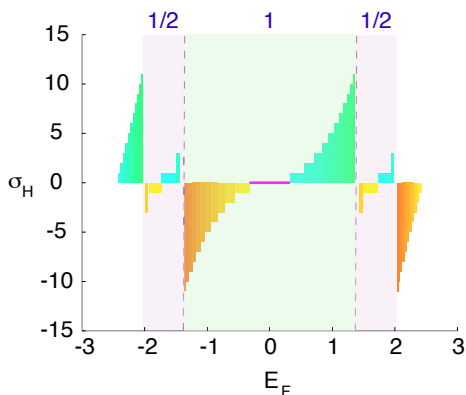


Figure 2: Hall conductivity $\sigma_H(E_F)$ as a function of the Fermi energy for $\Phi \approx 0.05$. Vertical dotted lines indicate the location of van Hove singularities (cf. Fig. 1 (d)).

(b) *Spin-orbit coupling.* An intrinsic spin-orbit (SO) coupling term, $H_{SO} = i\lambda_{SO} \sum_{\langle\langle ij \rangle\rangle} \alpha_{\beta} (\mathbf{d}_{ij}^1 \times \mathbf{d}_{ij}^2) \cdot \sigma_{\alpha\beta} c_{i\alpha}^{\dagger} c_{j\beta}$, has been introduced in Ref. [15] to predict the quantum spin Hall effect in a model described by a standard honeycomb lattice. Here λ_{SO} is the SO coupling strength, \mathbf{d}_{ij}^1 and \mathbf{d}_{ij}^2 are two NN vectors connecting the NNN sites i and j , and σ is the vector of Pauli matrices acting on the spin. This term opens a bulk gap in the energy spectrum that is associated to a non-trivial Z_2 index and hosts topologically protected helical edge states [15]. This NNN SO term has been generalized to other

\mathcal{P}_3	Γ_0	Γ_1	Γ_2	Γ_3	\prod_i	ν
Band 4	+1	-1	+1	-1	1	$\nu_4 = 1$
Band 3	-1	+1	-1	+1	1	$\nu_3 = 1$
Band 2	+1	-1	+1	-1	1	$\nu_2 = 1$
Band 1	+1	+1	-1	+1	-1	$\nu_1 = 1$

Table I: Parity-eigenvalue pattern at the four \mathcal{T} -invariant momenta Γ_i for the four different occupied bands. All the bulk gaps are associated with a non-trivial Z_2 index $\nu = 1$.

lattices exhibiting spin-1/2 relativistic fermions [9, 16], and systematically leads to non-trivial Z_2 phases. In lattices featuring effective spin-1 fermions, such as the Lieb or \mathcal{T}_3 lattices, the situation is more subtle. The NNN SO term leads to a trivial phase for the \mathcal{T}_3 lattice but a non-trivial phase for the Lieb lattice [3, 4, 17]. Therefore, the effect of the SO term on the ECH lattice, in which spin-1 and spin-1/2 excitations coexist, is *a priori* a non-trivial problem.

First, we show how the SO term affects the low-energy theory describing the two kinds of Dirac-Weyl fermions. In this limit the effective Hamiltonians are

$$h_{\mathbf{k}}^{1/2} = v_{1/2}(k_x \sigma_1 + k_y \sigma_2) - \frac{\sqrt{3}}{2} \alpha \lambda_{SO} \sigma_3 \quad (3)$$

$$h_{\mathbf{k}}^1 = v_1(k_x S_1 + k_y S_2) - 2\sqrt{3} \alpha \lambda_{SO} S_3 \quad (4)$$

where $\alpha = \pm$ is the spin index. We note that Eq. (3) holds for all the spin-1/2 Dirac species, namely for all \mathbf{K}_{\pm} at $f = 1/5, 4/5$. The SO term generates the same mass term for all the spin-1/2 relativistic excitations, and thus opens bulk gaps at the four independent spin-1/2 Dirac points. Two bulk gaps also appear in the vicinity of the spin-1 Dirac point (i.e. $f = 1/2$) with the flat band being preserved by the SO term.

We now compute the four Z_2 indices ν_N , with $N = 1, 2, 3, 4$ associated with the four bulk gaps opened by H_{SO} . Since the ECH lattice possesses inversion symmetry, the Z_2 topological invariant ν_N associated with the N th bulk gap can be easily evaluated through the formula [18, 19]

$$\prod_{i=0}^3 \prod_{m=1}^N \xi_{2m}(\Gamma_i) = (-1)^{\nu_N}. \quad (5)$$

In this expression, $\xi_{2m}(\Gamma_i) = \pm 1$ is the parity eigenvalue associated with the $2m$ -th occupied energy band, which is evaluated at one of the four \mathcal{T} -invariant momenta Γ_i . The latter can be expressed as $\Gamma_i = \hat{\mathbf{q}}_1 n_i/2 + \hat{\mathbf{q}}_2 m_i/2$, with $n_i, m_i = 0, 1$, where $\hat{\mathbf{q}}_1 = 2\pi/3(1, \sqrt{3})$ and $\hat{\mathbf{q}}_2 = 2\pi/3(1, -\sqrt{3})$. Choosing the site $\tau = 3$ inside the unit cell as the center of inversion, the parity operator acts as $\mathcal{P}_3[\psi_1(\mathbf{r}), \psi_2(\mathbf{r}), \psi_3(\mathbf{r}), \psi_4(\mathbf{r}), \psi_5(\mathbf{r})] = [\psi_1(-\mathbf{r} - \mathbf{b}_3), \psi_4(-\mathbf{r} + \mathbf{a}_1), \psi_3(-\mathbf{r}), \psi_2(-\mathbf{r} - \mathbf{a}_1), \psi_5(-\mathbf{r} - \mathbf{b}_2)]$, where $\psi_{\tau}(\mathbf{r})$ is the single-particle wavefunction defined at site τ . The eigenstates of H_{Γ_i} , as well as the parity eigenvalues of the occupied bands, are determined numerically, yielding the results presented in Table I. We find that the expression (5) gives $(-1)^{\nu} = -1$ for each bulk gap, indicating that the Z_2 phases

generated by the SO term are all non-trivial. Therefore, the spin-1 regime of the ECH lattice behaves similarly to the Lieb lattice [3, 4, 17].

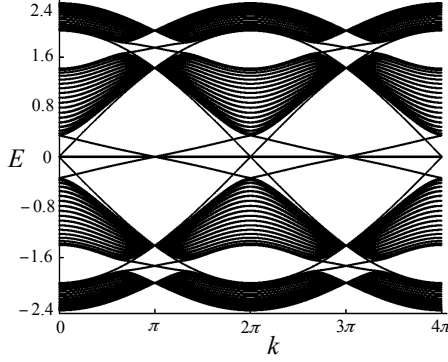


Figure 3: The energy spectrum $E = E(k)$, for an ECH lattice subject to an intrinsic SO coupling with periodic boundary conditions along one spatial direction shows the presence of helical edge states in the vicinity of both the spin-1/2 and the spin-1 regime.

To further confirm these results, we diagonalize the ECH lattice in the presence of the SO term and consider periodic boundary conditions along one spatial direction. In this cylindrical geometry, the energy spectrum features helical edge states within the four bulk gaps predicted by the non-trivial Z_2 index [9, 15, 16] (see. Fig. 3). We note that the dispersion relations $E(k)$ associated with the edge states at half-filling are similar to those obtained from the Lieb lattice [4, 17], further indicating the similarity between the spin-1 regimes of the ECH and Lieb lattices. In the vicinity of the spin-1/2 regime, i.e., $f = 1/5, 4/5$, the dispersion relation of the edge states is similar to those obtained in the Kagome lattice [9]. These results show that the SO term acts in a non-trivial way, both for the spin-1 and spin-1/2 regimes, indicating that the ECH lattice presents striking similarities with both the Kagome and the Lieb lattices. However, the presence of a SO term does not allow us to distinguish between the spin-1 and spin-1/2 regimes, as they would both give rise to the same quantum spin Hall effect.

(c) *Charge density waves (CDW)* Here we are interested in the fate of the spin-1/2 and spin-1 Dirac points, when a charge density wave term [9, 16], $H_{\mathbf{k}}^{CDW} = \text{diag}(\mu_1, \dots, \mu_5)$, is added in the ECH lattice, where the local chemical potentials μ_τ can be individually tuned. In the vicinity of the four spin-1/2 Dirac points K_\pm , we find that the low-energy terms corresponding to the CDW take the form

$$h(\mathbf{p})_{CDW}^{1/2} = -(A_x^l \sigma_1 + A_y^l \sigma_2 - A_z^l \sigma_3) + A_0 I, \quad f = \frac{1}{5} \quad (6)$$

$$h(\mathbf{p})_{CDW}^{1/2} = (A_x^l \sigma_1 + A_y^l \sigma_2 + A_z^l \sigma_3) + A_0 I, \quad f = \frac{4}{5} \quad (7)$$

where $A_x^l = (\mu_1 - \mu_5)l/4\sqrt{3}$, $A_y^l = (\mu_1 - 2\mu_3 + \mu_5)l/12$, $A_z^l = (\mu_2 - \mu_4)l/4$, $A_0 = (2\mu_1 + 3\mu_2 + 2\mu_3 + 3\mu_4 + 2\mu_5)/12$, and $l = \pm$ refers to the two Dirac points \mathbf{K}_\pm . Therefore when $\mu_2 = \mu_4$, i.e., $A_z^l = 0$, and similar to the results reported for

the Kagome lattice, we find that the CDW acts as an axial gauge field. Namely, a gauge potential \mathbf{A} which has opposite sign at two independent Dirac points [9, 16] with the low-energy Hamiltonians $h(\mathbf{p})^{1/2} = \sum_{\nu} v_{1/2} (k_\nu - \mathcal{A}_\nu^l) \sigma_\nu$, where $\mathcal{A}_\nu^l = A_\nu^l/v_{1/2}$ and $\mathcal{A}_\nu^+ = -\mathcal{A}_\nu^-$. In this case the impact of the gauge potential \mathcal{A}_ν^\pm on the spin-1/2 Dirac-Weyl fermions is to move the positions of their Dirac points inside the Brillouin zone. At a given filling, the displacement of the two Dirac points are opposite, since the gauge field is axial. Furthermore, these displacements are performed in opposite directions at fillings $f = 1/5$ and $f = 4/5$ (cf. Eq. (7)). In other words, if two Dirac cones come closer at $f = 1/5$ as the CDW is increased, the two cones at $f = 4/5$ will separate. When the CDW is sufficiently strong, the two approaching Dirac points at $f = 1/5$ will annihilate each other [20, 21], while the two Dirac points at $f = 4/5$ will survive. This process allows to destroy a pair of spin-1/2 species at a given filling while preserving the others.

In contrast, by expanding the Hamiltonian around the spin-1 Dirac point at Γ_0 , we find that the low-energy form of the CDW perturbation is more involved than for the spin-1/2 regime, and that it cannot be simply interpreted as a gauge field. Indeed, the low-energy limit of the CDW term cannot be written as a superposition of the three angular-momentum matrices $S_{x,y,z}$ which do not form a complete basis for 3×3 matrices. This interesting result indicates that the spin-1/2 and spin-1 regimes of the ECH lattice should react differently to the CDW, providing a mechanism for distinguishing them in an experiment.

The possibility to destroy and preserve the spin-1/2 and spin-1 fermions *individually*, using the CDW perturbation, is appealing. Here, we report several relevant configurations that achieve this goal.

- $\mu_2 = -\mu_4$ and $\mu_1 = \mu_3 = \mu_5$. In this case, the CDW acts as a staggered potential for the background honeycomb lattice. It destroys all the spin-1/2 Dirac points at \mathbf{K}_\pm and $f = 1/5, 4/5$ by opening trivial bulk gaps [15]. By setting $\mu_1 = \mu_3 = \mu_5$, the CDW do not perturb the localized states defined at the green sites of Fig. 1 (a): therefore, the flat band is preserved. Besides, we find that the spin-1 Dirac point at Γ_0 only survives for $\mu_2 = -\mu_4$ and $\mu_1 = \mu_3 = \mu_5 = 0$.
- $\mu_2 = \mu_4$ and $\mu_1 = \mu_3 = \mu_5$. In this case, $A_x^l = A_y^l = A_z^l = 0$ and $A_0^l \neq 0$, thus the spin-1/2 Dirac points are simply shifted in energy. Since $\mu_1 = \mu_3 = \mu_5$, the flat band is preserved but the spin-1 Dirac point at Γ_0 is destroyed (cf. above).
- $\mu_2 = \mu_4$ and arbitrary $\mu_{1,3,5}$. In this case, the CDW acts as a non-trivial axial gauge field and the spin-1/2 Dirac points move inside the Brillouin zone in opposite directions. Therefore, for small CDW, the spin-1/2 fermions are all preserved. For larger CDW, two fermions generally annihilate each other at $f = 1/5$ or $f = 4/5$ (the

displacements being oppositely performed at these fillings), in which case only one spin-1/2 regime survives. In addition, for arbitrary $\mu_{1,3,5}$ the flat band and the spin-1 Dirac fermion are destroyed.

Conclusions. We have investigated the ECH lattice where spin-1/2 and spin-1 Dirac-Weyl fermions were found to co-exist at different filling fractions. We explored several types of perturbations on the lattice which offer a powerful control over this rich system. It is certainly tempting to extend this scenario to include collisional interactions between the spins. This will not only allow for exotic new phases [22, 23] and applications of models such as the Kitaev anyonic model [24], but will also hopefully shed light on open questions at the forefront of condensed-matter physics.

Acknowledgements. ZL acknowledges the support from SUPA (Scottish Universities Physics Alliance). NG thanks the FRS-FNRS for financial support. PÖ acknowledges support from the Carnegie Trust for the Universities of Scotland.

[1] A. H. Castro Neto *et al*, Rev. Mod. Phys. **81**, 109 (2009).
 [2] X.-L. Qi and S.-C. Zhang, Rev. Mod. Phys. **83**, 1057 (2011).
 [3] D. Bercioux *et al*, Phys. Rev. A **80**, 063603 (2009); *ibid* **83**, 023609 (2011)
 [4] N. Goldman, D. F. Urban and D. Bercioux, Phys. Rev. A **83**, 063601 (2011)

[5] V. Apaja, M. Hyrkäs and M. Mannien, Phys. Rev. A **82**, 041402(R) (2010).
 [6] R. Shen *et al*, Phys. Rev. B **81**, 041410(R) (2010).
 [7] Z. Lan *et al*, Phys. Rev. B **84**, 165115 (2011).
 [8] H Watanabe, Y Hatsugai, and H Aoki, arXiv:1009.1959 (2010); B. Dóra, J. Kailasvuori, and R. Moessner, Phys. Rev. B **84**, 195422 (2011).
 [9] H.-M. Guo and M. Franz, Phys. Rev. B **80**, 113102 (2009).
 [10] A. Singha *et al*, Science **332**, 1173 (2011).
 [11] J. Dalibard *et al*, Rev. Mod. Phys. **83**, 1523 (2011)
 [12] M. Aidelsburger *et al*, Phys. Rev. Lett. **107**, 255301 (2011).
 [13] Hideo Aoki, Masato Ando, and Hajime Matsumura, Phys. Rev. B **54**, 17296(R) (1996).
 [14] K. S. Novoselov *et al*, Nature **438**, 197 (2005); Y. Zhang *et al*, Nature **438**, 201 (2005).
 [15] C. L. Kane and E. J. Mele, Phys. Rev. Lett. **95**, 146802 (2005).
 [16] A. Ruegg, J. Wen and G. A. Fiete, Phys. Rev. B **81**, 205115 (2010).
 [17] C. Weeks and M. Franz, Phys. Rev. B **82**, 085310 (2010).
 [18] L. Fu and C. L. Kane, Phys. Rev. B **76**, 045320 (2007).
 [19] T. L. Hughes, E. Prodan, and B. A. Bernevig, Phys. Rev. B **83**, 245132 (2011).
 [20] A. Bermudez *et al*, New J. Phys. **12**, 033041 (2010).
 [21] L. Tarruell *et al*, arXiv:1111.5020 (2011).
 [22] Z. Y. Meng *et al*, Nature **464**, 847 (2010).
 [23] W. Zhang, arXiv:1201.0722 (2012); W.-F. Tsai *et al*, arXiv:1112.5789 (2011);
 [24] A. Kitaev, Ann. Phys. **321**, 2 (2006).